POAC'13
Espoo, Finland

Proceedings of the 22nd International Conference on
Port and Ocean Engineering under Arctic Conditions
June 9-13, 2013
Espoo, Finland

MAPS FOR BRITTLE AND BRITTLE-LIKE FAILURE IN ICE

Carl E. Renshaw [1], Narayana Golding [2], Erland M. Schulson [2]

[1]Department of Earth Sciences, Dartmouth College, Hanover, NH 03755 USA

[2] Thayer School of Engineering, Dartmouth College, Hanover, NH 03755, USA

ABSTRACT

The strain rate and stress required for faulting in ice under low to moderate confinement are well understood and can be quantified in terms of independently measured materials parameters. Under high confinement, defined as confinement sufficient to suppress frictional sliding, brittle-like failure is still observed, even at pressure well below that required for faulting associated with phase transformations. While previous work has qualitatively suggested that high-confinement faults not associated with phase transformations, here termed P-faults, are likely associated with adiabatic instabilities, the failure map for P-faulting remains incomplete because of the lack of a quantitative understanding of the P-faulting terminal failure stress. We develop a new quantitative model for the P-faulting terminal failure stress that is consistent with recent experimental observations and then use this model to complete the failure map for compressive brittle and brittle-like failure of freshwater ice.

INTRODUCTION

The stability of engineered structures in ice-infested waters is limited by loads induced by interactions with ice. Kim et al. (2012) demonstrated that loads during ice-structure interactions are governed by compressive failure processes active under both high and low confinement. When ice is rapidly loaded under little to no confinement, where confinement is defined as the ratio of the least to the most principal compressive stresses acting in the plane normal to the incipient fault plane, compressive failure occurs via axial splitting (Wachter, Renshaw et al. 2008). Under slightly higher but still low confinement, failure occurs via shear faulting (Schulson, Iliescu et al. 1999). Because shear faulting involves the initiation, sliding, and interaction of microcracks (Brace 1964, Ashby and Hallam 1986, Horii and Nemat Nasser 1986), we term this type of failure process Coulombic (C) faulting and emphasize that it requires that confinement be sufficiently low to allow frictional sliding along microcracks (Schulson 2002). In the laboratory, low confinement failure processes during ice-structure/penetrometer interactions, as indicated by the initiation and growth of microcracks, are evident in the region remote from the contact area where the confinement ratio R is less ~0.3 (Kim, Golding et al. 2012).

Under higher confinement ratios, frictional sliding is suppressed, but localized failure is still observed, even at pressure well below that required for faulting associated with phase transformations (Kirby 1987, Schulson 2002). We refer to high-confinement localized failure that occurs in the absence of phase transformations as plastic or P-faults. By "plastic" in this context we mean volume-conserving deformation, the resistance to which is independent of the hydrostatic component of the stress tensor. In laboratory studies of ice-structure/penetrometer interactions, recrystallized grains are common in the region of high (R > 0.3) confinement near the contact area while microcracks are not (Kim, Golding et al.

2012). In laboratory specimens localized shear failure often is not evident, but localized failure under high confinement has been observed in the field. For example, thin sections taken from an iceberg after the 500 - 1500 ton floating ice mass impacted Grappling Island at a velocity V ~1.5 mm s^{-1} at T ~ 10 °C (Muggeridge and Jordaan 1999, Jordaan 2001) reveal narrow bands of finely recrystallized grains that are similar to P-faults observed in triaxially-loaded granular and columnar ice (Golding, Schulson et al. 2010, Golding 2012).

Given that both low and high confinement failure processes are involved in ice-structure interaction, a complete analysis of ice-structure interaction requires an understanding of both low and high confinement failure of ice. With regards to low confinement failure, previous work has quantified the strain rate and stress required for C-faulting in ice in terms of independently measured materials parameters (Renshaw and Schulson 2001). For high confinement failure, previous work has also defined the strains and strain rates necessary for P-faulting (Golding 2012), again in terms of non-adjustable parameters. However, work to date has not quantified a complete failure-mode map for high confinement failure, principally because our understanding of P-faulting failure stress remained incomplete. Here we develop such a map, based upon a new quantitative model for the P-faulting terminal failure stress that is consistent with recent experimental observations (Golding, Schulson et al. 2010, Golding 2012).

MODEL DEVELOPMENT

P-faulting

In P-faulting deformation is localized due to the instability that develops when thermal softening exceeds strain and strain rate hardening (Renshaw and Schulson 2004). The requirements are twofold; a critical local strain is required to generate sufficient heat, and a critical local strain rate is required to ensure approximately adiabatic conditions. By "local" we mean the strain and strain rate within the incipient plastic fault as opposed to the macroscopic "global" strain and strain rates obtained from measurements of displacement along boundaries. These requirements can be quantified and combined through a balance of the effects of strain and strain rate hardening and the effect of thermal softening, yielding the critical strain rate $\dot{\bar{\varepsilon}}_c$ required for P-faulting (Golding 2012, eqns. 1 and 2)

$$\dot{\bar{\varepsilon}}_c = \frac{-2\sqrt{2}a\kappa m w_f}{\ell w_d^2 \left(\partial\bar{\sigma}/\partial T\right)} \tag{1}$$

where m is the work- hardening exponent in the expression $\bar{\sigma} \propto \bar{\varepsilon}^m$, where $\bar{\sigma}$ and $\bar{\varepsilon}$ are the effective stress and strain, respectively (Golding, Schulson et al. 2010), a is a geometrical factor of order unity, κ is the thermal conductivity, w_f is the fault width, w_d is the characteristic length of heat diffusion, $\partial\bar{\sigma}/\partial T$ denotes thermal softening and ℓ is the characteristic length of the sample/body. In the laboratory where a single fault generally develops within sub-meter sized test specimens, ℓ is taken as the length of the specimen along the direction of shortening.

The effective stress required for P-faulting can be estimated by combining the critical strain rate $\dot{\bar{\varepsilon}}_c$ with a rate dependent plastic flow law to relate the critical global strain rate to the corresponding failure stress. At relatively low stresses the relationship between effective

stress $\bar{\sigma}$ and effective strain rate $\dot{\bar{\varepsilon}}$ rock is typically described using an Arrhenius power-law equation of the form

$$\dot{\bar{\varepsilon}} = A_p \bar{\sigma}^{n_p} e^{-Q_p/(RT)} \tag{2}$$

where A_p is a materials property, Q_p is an apparent activation energy, R is the gas constant, and n_p is the stress exponent. At higher stresses the creep-rate-limiting process is thought to transition from climb-controlled to glide-controlled dislocation motion (Frost and Ashby 1982). The power-law relationship between effective stress and effective strain rate may break down in this high-stress creep regime and deformation may instead be characterized by an exponential flow law of the form $\dot{\bar{\varepsilon}} = A_e e^{\beta\bar{\sigma}} e^{-Q/(RT)}$, where A_e and β are materials properties (Evans and Goetze 1979, Tsenn and Carter 1987). The transition from a low-stress power law to a high-stress exponential flow law can by described by a single hyperbolic creep law of the form (Garofalo 1963, Wong and Jonas 1968)

$$\dot{\bar{\varepsilon}} = A_h \left[\sinh\left(\alpha\bar{\sigma}\right)\right]^{n_h} e^{-Q_h/(RT)} \tag{3}$$

where A_h is a materials property, Q_n is an apparent activation energy, n_h is the stress exponent, and the parameter α is the reciprocal of the effective stress at which low and high stress creep contribute equally to the global creep rate. For values of $\alpha\bar{\sigma}$ less than about 0.8, this expression reduces to the Arrhenius power-law equation with $A_h = A_p / \alpha^n$. For $\alpha\bar{\sigma}$ greater than about 1.2 this expression reduces to an exponential flow law (Barnes, Tabor et al. 1971).

Combining Eqns. (1) and (2), the P-faulting failure stress when ductile deformation is governed by an Arrhenius power-law is

$$\bar{\sigma} = \left(\frac{-2\sqrt{2} a \kappa m w_f}{A_p l w_d^2 \left(\partial\bar{\sigma}/\partial T\right)} \right)^{1/n_p} e^{Q_p/n_p RT} \tag{4}$$

Similarly, if ductile deformation is governed by the hyperbolic creep law, combining eqn. (1) and (3) gives the P-faulting failure stress as

$$\bar{\sigma} = \frac{1}{\alpha} \sinh^{-1} \left[\left(\frac{-2\sqrt{2} a \kappa m w_f}{A_h l w_d^2 \left(\partial\bar{\sigma}/\partial T\right)} \right)^{1/n_h} e^{Q_h/n_h RT} \right] \tag{5}$$

C-faulting

The strain rate that marks the ductile-brittle transition under conditions that lead to C-faulting can be estimated following the analysis of Schulson et al., (Schulson, Iliescu et al. 1999) and of Renshaw & Schulson (Renshaw and Schulson 2001). Accordingly, and building on experimental observations, the analysis suggests that C-faulting initiates owing to the bending-induced failure of slender microcolumns created from sets of secondary cracks that emanate from one side of a sliding primary crack. The C-faulting transitional strain rate is then given by (Renshaw and Schulson 2001)

$$\dot{\varepsilon}_c^C = \frac{25K_{Ic}^3 A_p e^{-Q_p/(RT)}}{d^{3/2}[(1-R_c)-\mu(1+R_c)]} \qquad R < \frac{1-\mu}{1+\mu} \tag{6}$$

where $\dot{\varepsilon}_c^C$ is the minimum strain rate required for C-faulting, K_{IC} is the fracture toughness, d is the grain size, μ is the friction coefficient, R_c is the confinement ratio, and the material parameters A_p and Q_p are those for low-stress power-law creep.

Table 1. Deformation parameters*

Temperature (°C)	0 to -2**	-2 to -8	-8 to -45
Hyperbolic creep law			
A_h (s^{-1})	2.5 x 10^{19}	4.6 x 10^{18}	2.7 x 10^{10}
α (MPa^{-1})	0.279	0.279	0.262
n_h	3.14	3.14	3.05
Q_h (kJ mol^{-1})	120	120	78.1
Low stress power law creep			
A_p (MPa^{-n} s^{-1})			4.7 x 10^8
n_p			3
Q_p (kJ mol^{-1})			78.1
High stress power law creep			
A_p (MPa^{-n} s^{-1})			8.8 x 10^6
n_p			4.8
Q_p (kJ mol^{-1})			74.1
C-faulting			
K_{Ic} (MPa $m^{1/2}$)			0.1
μ***			0.5 (-10 °C)
			0.65 (-40 °C)

* Hyperbolic creep law parameters from Barnes et al. (1971)
**Parameters at these temperatures are estimated
*** From Fortt and Schulson (2007)

MODEL PARAMETERIZATION

Parametric values for C-faulting are summarized in Table 1 and are identical to those used previously (Renshaw and Schulson 2001). In Fig. 1 we compare the Arrhenius power-law and hyperbolic creep law to experimental observations of steady state plastic flow of nominally ~1 mm grain size freshwater ice at temperatures from -48 °C to -2 °C under applied stresses from 0.05 MPa to 20 MPa.; i.e., over experimental ranges likely to bracket practical interest to the ice-interaction problem. Parametric values for the hyperbolic creep law are those given by Barnes et al. (Barnes, Tabor et al. 1971) and are summarized in Table 1. In general the model fit is good and well captures the transition from low- to high-stress creep, which occurs at an effective stress of $1/\alpha \approx 3.7$ MPa. In the inset of Figure 1 we re-plot the high-stress plastic flow data, i.e, the experimental data having an effective stress greater than the transitional stress $(1/\alpha)$. Also shown in the inset are the predictions of the hyperbolic creep law with the parameters from Barnes et al. (Barnes, Tabor et al. 1971) (solid line) and a best-fit high-stress power-law creep law (dashed line). Best-fit model parameters for the high-stress creep law are given in Table 1. Over the range of the available data, both models are nearly equivalent and fit the data nearly equally well. Note, however, that the two models diverge at higher stresses; at typical P-faulting failure stresses (~20 MPa at -10 °C) the strain

rates predicted by the hyperbolic creep law are about two orders of magnitude greater than those predicted by the high-stress creep law.

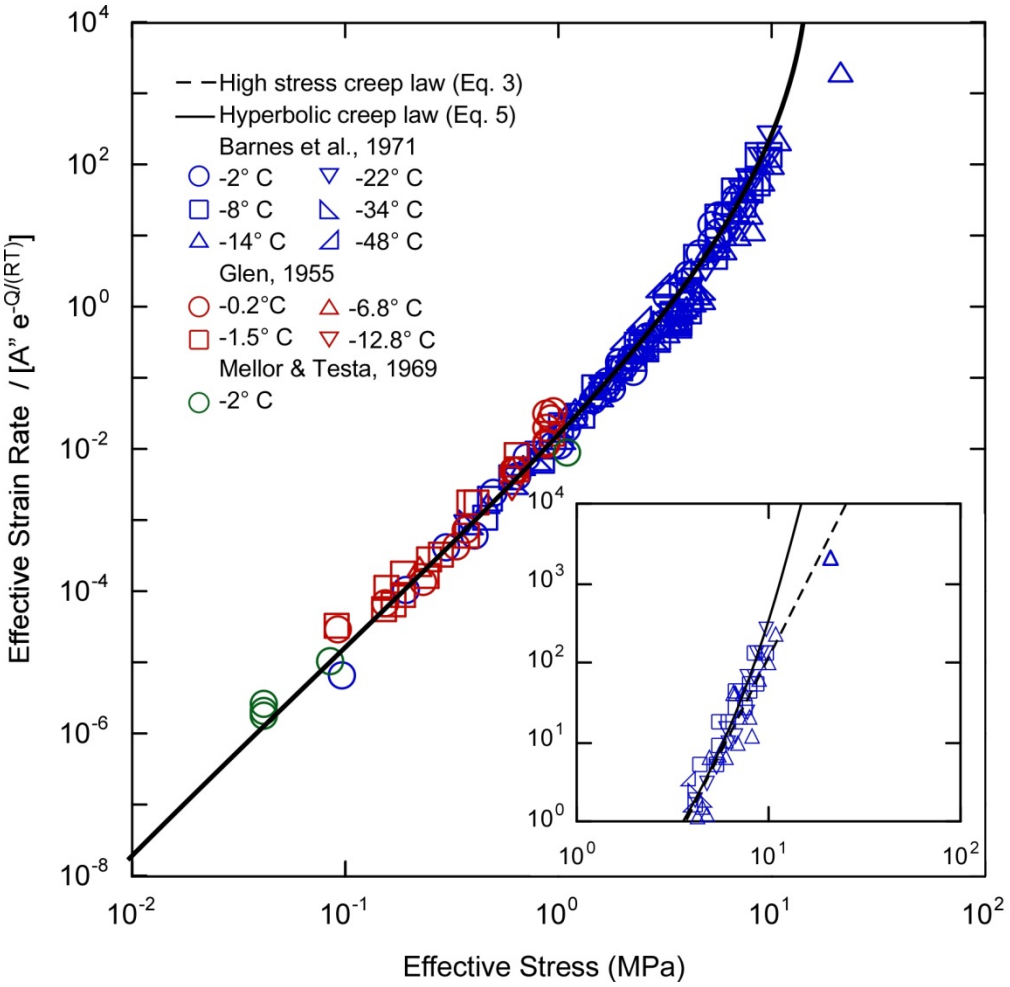

Figure 1. Experimentally observed stress dependence of the strain rate of nominally 1 mm grain size freshwater ice compared to the high stress and hyperbolic creep laws. Inset is an enlarge view of the high stress data. Data from (Glen 1955, Mellor and Testa 1969, Barnes, Tabor et al. 1971).

Assuming that either the hyperbolic or the high-stress creep law applies, thermal softening can be estimated by differentiating these expressions with respect to temperature. For the hyperbolic creep law, this yields:

$$\frac{\partial \bar{\sigma}}{\partial T} = -\frac{Q_h \left(\dot{\bar{\varepsilon}}^{global} / A_h \right)^{1/n_h} e^{\left(Q_h/(n_h RT)\right)}}{\alpha n_h RT^2 \sqrt{\left(\dot{\bar{\varepsilon}}^{global} / A_h \right)^{2/n_h} e^{\left(2Q_h/(n_h RT)\right)} + 1}} \tag{9}$$

while for high-stress power-law creep the thermal softening is

$$\frac{\partial \bar{\sigma}}{\partial T} = \frac{-Q_p}{n_p R T^2} e^{-Q_p/(n_p RT)} \left(\frac{\dot{\varepsilon}^{global}}{A_p} \right)^{1/n_p} \tag{10}$$

The thermal softening predicted by the above expressions is used with Eq. (1) to solve for the critical strain rate required for P-faulting. In practice these calculations are done iteratively to ensure that the critical global strain rate is self-consistent; that is, by adjusting an assumed critical global strain rate used to determine the thermal softening until the assumed strain rate matches that predicted by Eq. (1). Finally, having obtained the critical strain rate, the corresponding creep law is used with this critical strain rate to determine the effective stress required for P-faulting (Eq. 4 or 5).

FAILURE MODE MAPS

Confinement versus strain rate

In Fig. 2 we compare the ductile-to-brittle transitional strain rates predicted by our C-faulting model and by our high-stress power-law creep law model for P-faulting to the experimental data for granular and columnar S2 ice as reported by Golding et al. (Golding, Schulson et al. 2010, Golding 2012) . Included are supplemental data for axial splitting from Watcher et al. (Wachter, Renshaw et al. 2008) and data for low-confinement ductile failure from Schulson & Buck (Schulson and Buck 1995). In all cases loads applied to S2 ice were applied perpendicular to the long axis of the columns. The main graph shows the observations and model predictions for T = -10 °C, while the inset shows the observations and model predictions for T = -40 °C. Here the transitional strain rates are shown as a function of the confinement ratio, R_c. In general the experimental data are consistent with the theoretical predictions at both temperatures, particularly for granular ice. The most notable discrepancy is that the critical applied strain rate at which globally distributed ductile deformation transitions to P-faulting in columnar ice is about a factor of four lower than that observed for granular ice and predicted using the high-stress creep law.

Strain rate versus terminal failure stress

It is also possible to map deformation mode, at a given temperature, with respect to the terminal effective stress, either as a function of confinement (Renshaw and Schulson 2001) or as a function of applied strain rate. As an example, in Fig. 3 we plot the experimentally observed terminal failure stresses of granular and columnar ice at T = -10 °C and R_c = 0.5 as a function of applied strain rate (Golding, Schulson et al. 2010, Golding 2012). Also shown are the maximum effective stresses predicted using, in the ductile regime, the low-stress creep law. In the P-faulting regime we predict the failure stress by using the applied strain rate to estimate the thermal softening via the high-stress creep law, using this estimated thermal softening to determine an effective global strain rate using Eq. (1), and then relating this effective global strain rate to the corresponding effective stress using the high-stress creep law (Eq. 4). The predicted maximum effective stresses agree well with the experimental observations in both the globally ductile and the P-faulting regimes. Note also the while the applied strain rate at which deformation transitions from ductile to P-faulting differs by a factor of four between columnar and granular ice, the maximum effective stresses in both materials are similar and both are well predicted using our P-faulting model with the high-stress creep law. The similarity in terminal failure stresses of columnar and granular ice, despite the fact that columnar ice is nominally plastically anisotropic in comparison to the plastic isotropy of granular ice, could reflect the recrystallization of columnar ice into a more granular microstructure just prior to terminal failure. While we were unable to

experimentally observe such a transition in microstructure prior to failure (Golding, Schulson et al. 2010, Golding 2012), this might be an artefact of the limited temporal resolution of our observations.

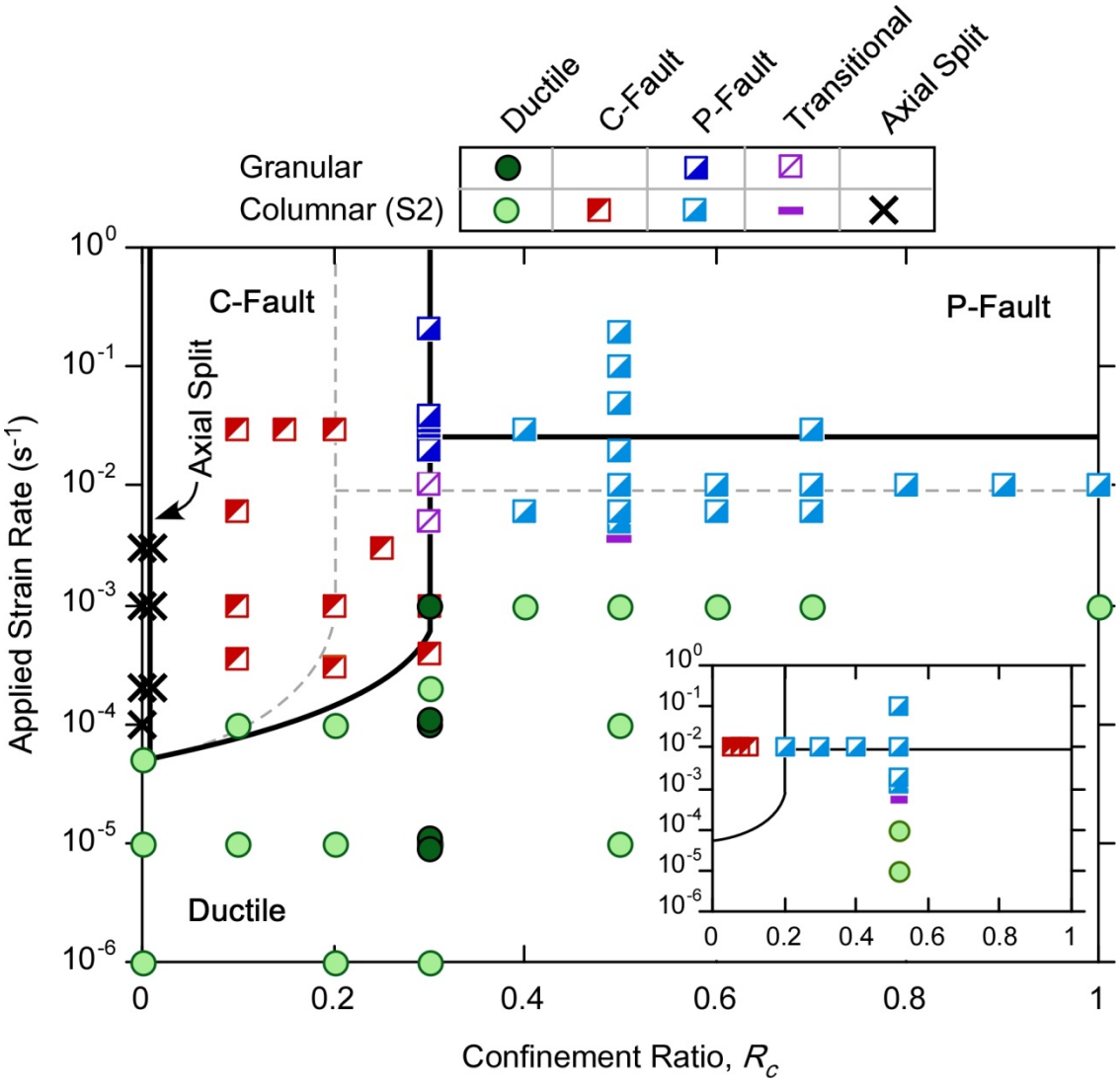

Figure 2. Mode of failure observed and predicted as a function of confinement and applied strain rate. Lines indicates brittle ductile transition as predicted under low confinement by Renshaw and Schulson and under high confinement by Eq. (1) with the high stress power-law creep law. Solid line are transitions predicted for T = -10 °C, dashed lines for T = -40 °C. Experimental data from experiments on granular and freshwater ice where T = -10 °C.

DISCUSSION

The localization of deformation resulting in brittle and brittle-like failure of ice is a consequence of a material instability. Under low confinement (but high enough to activate C-faulting rather than axial splitting), the root instability leading to brittle failure appears to be the failure of slender columns created between sets of secondary cracks that stem in the direction of shortening from sliding, primary cracks (Schulson, Iliescu et al. 1999). Under confinements sufficient to prevent frictional sliding other types of material instabilities can still localize deformation and result in brittle-like failure, such as when pressures are sufficient to drive phase transformations (Kirby 1987). While that idea of adiabatic instability has been around for decades (e.g., Orowan 1960) and is well known in works on metals (e.g.,

Basinski 1957), on polymers (e.g., Winter 1975) and on metallic glasses (e.g., Perez-Prado, Hines et al. 2001), only recently has the idea been explored, at least experimentally, in more nominally brittle crystalline materials such as ice. Here we have extended recent experimental observations of brittle-like failure of ice under high confinement that are qualitatively consistent with adiabatic instabilities (Golding, Schulson et al. 2010, Golding 2012) to demonstrate that these observations are also quantitatively consistent with adiabatic instabilities that result in P-faults. In particular, the quantitative expressions for the P-faulting failure stress presented here allow for the completion of the failure mode map for ice loaded under compression. Examples of these maps are shown in Figs. (2) and (3).

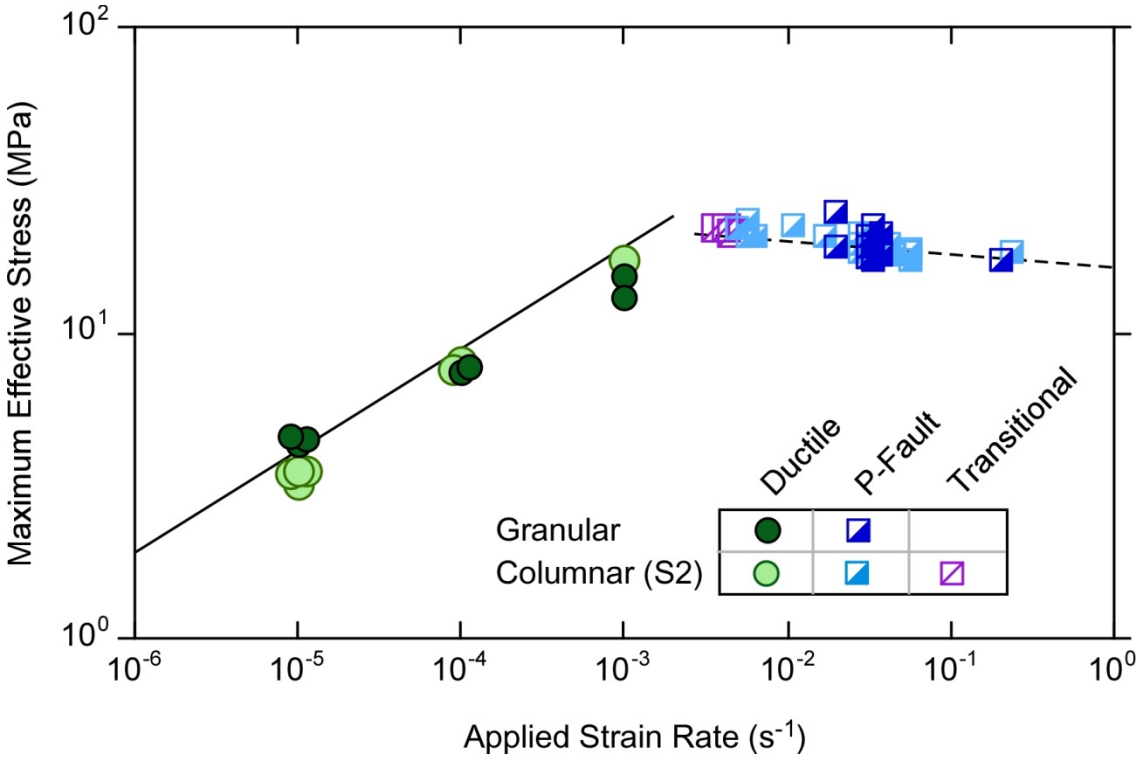

Figure 3. Mode of failure observed and predicted as a function of applied strain rate and effective stress at failure at T = -10 °C and R = 0.5. Lines indicate failure stress predicted using either the low stress creep law (solid line) or Eq. (9) with the high stress creep law (dashed line). Experimental data from Golding et al. (Golding, Schulson et al. 2010, Golding 2012).

Returning to the stability of engineered structures in ice-infested waters, a key result from this work is that the increase in terminal failure stress of ice under high confinement with increasing strain rate is bounded by P-faulting. That is, under confinement ratios sufficient to suppress frictional sliding (and thus inhibit C-faulting), the terminal failure stress of ice does not continue to increase with applied strain rate as predicted by the low-stress creep law (Eq. 2). Instead, in both columnar S2 and granular ice at temperatures between -40 and -10 °C, at strain rates around 10^{-2} s^{-1}, deformation transitions from being globally distributed to being localized within a plastic fault. This means that in modelling ice forces acting on vertically-sided engineered structures from physical principles, it is important to take into account the various modes of compressive failure that can be induced by the varying degree of confinement within the contact zone.

Acknowledgements – This work was supported by NFS grants EAR-0911071 and EAR-071019.

REFERENCES

Ashby, M. F. and S. D. Hallam (1986). "The Failure of Brittle Solids Containing Small Cracks under Compressive Stress States." Acta Metallurgica **34**(3): 497-510.

Barnes, P., D. Tabor and J. F. C. Walker (1971). "The friction and creep of polycrystalline ice." Proc. Royal Soc. London A **324**: 127-155.

Basinski, Z. S. (1957). "The instability of plastic flow at very low temperatures." Proc. R. Soc. London Ser. A. **240**: 229-242.

Brace, W. F. (1964). Brittle fracture of rock. State of Stress in the Earth's Crust. W. R. Judd. New York, Elsevier**:** 111-178.

Evans, A. G. and C. Goetze (1979). "The temperature variation of hardness of olivine and its implication for polycrystalline yield stress." J. Geophys. Res. **84**(B10): 5505-5524.

Frost, H. J. and M. F. Ashby (1982). Deformation-Mechanism Maps. Oxford, Permagon Press.

Garofalo, F. (1963). "An empirical relation defining the stress dependence of minimum creep rate in metals." Trans. Met. Soc. AIME **227**: 351-359.

Glen, J. W. (1955). "The creep of polycrystalline ice." Proc. R. Soc. London Ser. A. **228**(1175): 519-538.

Golding, N., E. M. Schulson and C. E. Renshaw (2010). "Shear faulting and localized heating in ice: The influence of confinement." Acta Materialia **58**(15): 5043-5056.

Golding, N., Schulson, E.M., Renshaw, C.E. (2012). "Shear localization in ice: Mechanical response and microstructural evolution of P-faulting." Acta Materialia **60**(8): 3616-3631.

Horii, H. and S. Nemat Nasser (1986). "Brittle Failure in Compression - Splitting, Faulting and Brittle-Ductile Transition." Philosophical Transactions of the Royal Society of London Series a-Mathematical Physical and Engineering Sciences **319**(1549): 337-374.

Jordaan, I. J. (2001). "Mechanics of ice-struture interaction." Eng. Fracture Mech. **68**: 1923-1960.

Kim, E., N. Golding, E. M. Schulson, S. Loset and C. E. Renshaw (2012). "Mechanisms governing failure of ice beneath a spherically-shaped indenter." Cold Regions Sci. Tech. **78**: 46-63.

Kirby, S. H. (1987). "Localized polymorphic phase transformations in high-pressure faults and applications to the physical mechanism of deep earthquakes." J. Geophys. Res. **92**(B13): 13,789-713,800.

Mellor, M. and R. Testa (1969). "Creep of ice under low stress." J. Glaciology **8**: 147-152.

Muggeridge, K. J. and I. J. Jordaan (1999). "Microstructural change in Ice III. Observations from an iceberg impact zone." J. Glaciology **45**: 449.

Orowan, E. (1960). "Mechanism of seismic faulting." Geol. Soc. Am. Mem. **79**: 323-345.

Perez-Prado, M. T., J. A. Hines and K. S. Vecchio (2001). "Microstructural evolution in adiabatic shear bands in Ta and Ta-W alloys." Acta materialia **49**: 2905-2917.

Renshaw, C. E. and E. M. Schulson (2001). "Universal behaviour in compressive failure of brittle materials." Nature **412**(6850): 897-900.

Renshaw, C. E. and E. M. Schulson (2004). "Plastic faulting: Brittle-like failure under high confinement." Journal of Geophysical Research-Solid Earth **109**(B9): B09207.

Schulson, E. M. (2002). "Compressive shear faults in ice: plastic vs. Coulombic faults." Acta Materialia **50**(13): 3415-3424.

Schulson, E. M. and S. E. Buck (1995). "The Ductile-to-Brittle Transition and Ductile Failure Envelopes of Orthotropic Ice under Biaxial Compression." Acta Metallurgica Et Materialia **43**(10): 3661-3668.

Schulson, E. M., D. Iliescu and C. E. Renshaw (1999). "On the initiation of shear faults during brittle compressive Failure: A new mechanism." Journal of Geophysical Research-Solid Earth **104**(B1): 695-705.
Tsenn, M. C. and N. L. Carter (1987). "Upper limits of power law creep of rocks." Tectonophysics **136**: 1-26.
Wachter, L. M., C. E. Renshaw and E. M. Schulson (2008). "Transition in brittle failure model in ice under low confinement." Acta Materialia **57**(2): 345-355.
Winter, R. E. (1975). "Adiabatic shear of titanium and polymethylmethacrylate." Philos. Mag. **31**(4): 765-773.
Wong, W. A. and J. J. Jonas (1968). "Aluminum extrusion as a thermally activated process." Trans. Met. Soc. AIME **242**: 2271-2280.